Phenotyping murine models of non-alcoholic fatty liver disease through metabolic profiling of intact liver tissue

Jeremy F.L Cobbold, Quentin M Anstee, Robert D. Goldin, Horace R.T. Williams, Helen C. Matthews, Bernard V. North, Nathan Absalom, Howard C. Thomas, Mark R. Thursz, Roger D. Cox, et al.

Clinical Science Immediate Publication. Published on 12 Aug 2008 as manuscript CS20080159

PHENOTYPING MURINE MODELS OF NON-ALCOHOLIC FATTY LIVER DISEASE THROUGH METABOLIC PROFILING OF INTACT LIVER TISSUE.

J.F.L. Cobbold[1,5], Q.M Anstee[1,3], R.D. Goldin[2], H.R.T. Williams[1,5], H.C. Matthews[1,3], B.V. North[4], N. Absalom[3], H.C. Thomas[1], M.R. Thursz[1], R.D. Cox[3], S.D. Taylor-Robinson[1], I.J. Cox[5].

[1]Department of Hepatology and Gastroenterology and [2]Department of Histopathology, Imperial College London, St Mary's Hospital Campus, London, U.K.
[3]MRC Mammalian Genetics Unit, MRC Harwell, Oxfordshire, U.K.
[4]Statistical Advisory Service, Imperial College London, South Kensington Campus, London, UK.
[5]Imaging Sciences Department, Imperial College London, Hammersmith Hospital Campus, London, U.K.

Short title: Phenotyping hepatic steatosis in mouse

Key Words: Steatohepatitis, NAFLD, spectroscopy, NMR, Diabetes

Corresponding Author/Reprint Requests:
Dr Jeremy F.L. Cobbold
Robert Steiner MR Unit
Imperial College London
Hammersmith Hospital Campus
Du Cane Road
London
W12 0HS
UK
Telephone: 020 8383 5856
Fax: 020 8383 3038
Email: j.cobbold@imperial.ac.uk

Main text: 4054 words, abstract: 201 words

Clinical Science Immediate Publication. Published on 12 Aug 2008 as manuscript CS20080159

Abstract

Non-alcoholic fatty liver disease (NAFLD) is a common cause of chronic liver disease, associated with the metabolic syndrome. Effective techniques are needed to investigate the potential of animal models of NAFLD. This study aimed to characterise murine models of NAFLD by metabolic profiling of intact liver tissue.

Mice of three strains (BALB/c, C3H and the novel mutant, Gena/263) were fed a control or high fat diet. Biometric, biochemical and histological analysis demonstrated a spectrum of NAFLD from normal liver to steatohepatitis. Metabolic profiling of intact liver tissue, using magic angle spinning proton magnetic resonance spectroscopy (MAS MRS), showed an increase in total lipid-to-water ratio, a decrease in polyunsaturation indices and a decrease in total choline with increasing disease severity. Principal components analysis and partial least squares discriminant analysis showed separation of each model from its control and of each model from the total dataset. Class membership from the whole dataset was predicted with 100% accuracy in 6 of 8 models. Those models with steatosis discriminated from those with steatohepatitis with 100% accuracy.

The separation of histologically-defined steatohepatitis from simple steatosis is clinically important. Indices derived from ^{1}H MAS MRS studies may inform subsequent *in vivo* MRS studies at lower field strengths.

Clinical Science Immediate Publication. Published on 12 Aug 2008 as manuscript CS20080159

Introduction

Non-alcoholic fatty liver disease (NAFLD) represents a spectrum of liver disease encompassing steatosis (fatty change), non-alcoholic steatohepatitis (NASH) and cirrhosis in the absence of alcohol abuse[1]. Population studies show that NAFLD is strongly associated with insulin resistance, type II diabetes mellitus, hypertension, obesity and dyslipidaemia[2-4]. The pathogenic mechanisms remain poorly understood and are difficult to study in humans[5]. While an estimated 10-24% of adults worldwide have a degree of hepatic steatosis[6], only a small proportion of these go on to develop progressive disease, characterised histologically by steatohepatitis with fibrosis. In order to target therapy to the appropriate patients there is a need for accurate, well-validated, methods to analyse hepatic lipid content and metabolism.

Magnetic resonance spectroscopy (MRS) provides information about the biochemical composition of tissues both *in vivo* and *in vitro*. *In vivo*, the technique has been used to assess the prevalence of NAFLD[7]; recently, more detailed information on lipid composition has been reported[8]. *In vitro*, MRS has been applied to the study of liver tissue extracts in obese rats[9] and urine and plasma from mice with features of NAFLD[10;11]. *In vitro* proton magic angle spinning (^{1}H MAS) MRS allows simultaneous analysis of lipid and aqueous compartments of intact solid tissue, resembling *in vivo* findings more closely than tissue extracts. In addition, ^{1}H MAS MRS requires a smaller mass of tissue for analysis compared to extracts[9;12], and enables histological evaluation of the sample following analysis[13]. ^{1}H MAS MRS has been applied to metabolic profiling in liver and other tissues from animal models and from humans[10;12;14-17].

Much of our understanding of the pathogenesis of NALFD is based on research using animal models[1]. No existing model exhibits the entire NAFLD phenotype. Many differ pathologically from human disease in all but superficial histological appearance. Thus, research is hampered by the lack of reliable models of progressive steatohepatitis that accurately reflect the human disease. Currently, the phenotyping of such models is reliant on physical observation, indirect biochemical assay and histopathology, all of which are time-consuming. In addition, subtle changes in metabolism and hepatic disease severity may not be detected using conventional techniques. Liver histology may be used to document overt features of NAFLD, such as the presence of hepatocellular lipid droplets, inflammation and fibrosis. Histological assessment is semi-quantitative and involves a degree of subjectivity in interpretation. There is a requirement for robust techniques to phenotype rapidly and categorise the output of programs that develop new models of NAFLD. In particular, there is a need to identify animals which exhibit the characteristics of more advanced disease, including steatohepatitis. Accordingly, the aims of this study were:

1. To characterise murine models of NAFLD using ^{1}H MAS MRS of intact liver tissue.
2. To assess the predictive value of multivariate models to determine the strain and diet for each mouse on the basis of ^{1}H MAS MRS differences.
3. To compare MR spectral differences between histologically characterised normal liver, steatosis and steatohepatitis.

Clinical Science Immediate Publication. Published on 12 Aug 2008 as manuscript CS20080159

Materials and Methods:

Animals

The study was approved by the local ethics committee and performed in accordance with the Animal (Scientific Procedures) Act 1986. Mice were housed under standard conditions (12 hour light/dark cycle, temperature 21±2°C, humidity 55±10%) and provided with food and access to drinking water *ad libitum*. Two inbred strains of mice, known to differ in susceptibility to dietary induced NAFLD, C3H/HeH (sensitive) and BALB/cAnNCrl (resistant) were used in these studies (each group, n = 6)[11]. In addition, a recently described genetic model of NASH maintained on a C3H/HeH background, Gena/263 *"Buttermouse"*, was studied (each group, n = 6-10). The Gena/263 model was identified using a phenotype-driven n-ethyl-n-nitrosurea (ENU) mutagenesis screen for impaired glucose tolerance and histological/biochemical evidence of steatohepatitis[18]. Male animals were randomised at age 6 weeks to receive either control diet (CD) or a nutritionally replete high fat diet (HFD). Control diet (SDS, Witham, UK) contained 4% fat by mass (11.5% of kcal) and the HFD (Research Diets Inc., New Brunswick, USA) contained 24% fat by mass (45% of kcal). [Dietary constituents are detailed in supplementary table 1].

The animals remained on the allocated diet for the remainder of the study. Body weight was measured at age 6, 20 and where applicable 36 weeks. Glucose tolerance assessed using an intraperitoneal glucose tolerance test (IPGTT) at age 12 weeks. Mice were culled by exsanguination under terminal anaesthesia at one of two time points, aged 20 or 36 weeks.

The liver was excised and half was snap-frozen in liquid nitrogen prior to storage at -80ºC, while the remainder was placed in 10% formalin. Formalin-fixed tissue was processed into paraffin wax and the sections were stained with haematoxylin & eosin, prior to histological examination by a histopathologist blinded to the phenotypic data, using the well validated NASH Clinical Research Network semi-quantitative scoring system for cellular morphology, inflammation and fibrosis[19].

Clinical Science Immediate Publication. Published on 12 Aug 2008 as manuscript CS20080159

Magnetic Resonance Spectroscopy studies
Two samples were analysed from each liver (mean sample mass 15.3mg, sd 2.9mg). Freshly thawed liver tissue was placed into XC4 Kel-F sealing cells (Doty Scientific Inc., Columbia, South Carolina, USA).

Proton MAS MRS experiments were carried out using a MAS probe (Doty Scientific Inc.) interfaced with a JEOL Eclipse 500+ spectrometer (JEOL (UK) Ltd, Welwyn Garden City, UK) and an 11.75T superconducting magnet (Oxford Instruments, Oxford UK). Samples were spun at 4000Hz and kept at 4ºC to minimise sample degradation during data acquisition[15]. A pulse and collect sequence (repetition time (TR) 10s, acquisition time 2.2s, 32 data collects) was used to derive a fully relaxed spectrum without suppression of the water resonance, the "total signal spectrum". A pulse and collect with a water presaturation sequence (TR 5s, acquisition time 2.2s, 64 data collects) provided water suppression, producing a spectrum dominated by lipid. A Carr-Purcell-Meiboom-Gill (CPMG) spin-echo pulse sequence with water presaturation (echo time 40ms, TR 5s, acquisition time 2.2s, 128 data collects) was employed to suppress macromolecular signal (mainly lipid) and emphasize lower molecular weight metabolite signals. In particular, this enabled the resolution and quantitation of the resonances within the total choline region. 32K data points were acquired for each spectrum with a spectral width of 15kHz[20]. The overall time for data acquisition was 35 minutes.

Data analysis and interpretation
Spectra were processed using KnowItAll® Informatics System v7.8 (Bio-Rad, Philadelphia, USA). Free induction decays were zero-filled by a factor of 2 and multiplied by an exponential windows function with a 1Hz line-broadening function prior to Fourier transformation. Spectral resonances were assigned according to the published literature [12;14-16]. Analysis was divided into hypothesis-generating multivariate analysis and biologically relevant conventional analysis of specific metabolites.

The spectral range of δ0-10.0ppm was analysed, including the water region for the pulse and collect sequences and excluding the region containing the residual water resonance (δ4.8-5.2ppm) in the sequences with water-presaturation. Spectra were scaled to the sum of the total spectral integral (water included for sequences *without* water suppression and excluded for those *with* water presaturation) to enable relative quantitative analysis of metabolites between samples.

Multivariate data analysis
The ^{1}H MAS MR spectrum from intact liver tissue demonstrated numerous identifiable resonances or peaks corresponding to specific metabolites (Figure 1). Accordingly, multivariate data-reduction techniques were applied in order to use information from the whole spectrum, and to determine which peaks contributed to the metabolic variation between individual samples and between groups of samples.

MR spectra acquired using the pulse and collect sequence with water presaturation were divided into small regions ("buckets") of 0.04±0.02ppm, representing specific metabolite functional groups, placed using an "intelligent bucketing" algorithm in the Knowitall® software. The integral of each bucket was then quantified and expressed as a proportion of the total spectral integral.

Unsupervised multivariate factor analysis was performed using principal components analysis (PCA) to assess clustering and the presence of outliers. PCA is an unbiased

technique, which is independent of any classifying information (such as strain) and the output summarises the metabolite variation within the dataset as a whole. Each principal component represents a combination of peaks, representing metabolites, expressed as a vector. The principal components are combined orthogonally, avoiding duplication or redundancy of information. Scores plots show the position of the samples in the newly defined multidimensional space, where the axes represent each orthogonal principal component. Examination of the loadings plots allows identification of those metabolites which predominantly account for variability within the dataset.

Supervised analysis was performed using partial least squares discriminant analysis (PLS-DA) to investigate factors associated with class membership, with the Pirouette v4.0 software package (Infometrics, Washington, USA). Here, the classifying information is included in the analysis, so the output summarises the MR spectral (metabolic) differences between the groups. Orthogonal signal correction (OSC) is a filtering technique applied to PLS-DA analyses to remove variation in the spectra, which is unrelated to the defined conditions[21]. To determine the predictive power of the model, cross-validation was performed by leaving out each sample in turn (a leave-one-out algorithm), and a model was constructed from the remaining samples to predict the class membership of the excluded sample. Such an algorithm makes best use of a small dataset, where a separate validation dataset is not possible. The Q^2 value indicates the validity of the discrimination, with values >0.05 considered significant[22;23].

Examination of spectral resonances

In order to examine the specific differences between metabolite ratios of prior interest and those identified in the loadings plots, peak integrals (proportional to the total quantity of the metabolite in the sample) were measured. The lipid:water ratio was derived from the pulse and collect spectra without water suppression, both as the sum of the integrals of all the fatty acid proton resonances and as the methylene proton:water peak expressed as a percentage. The polyunsaturated to monounsaturated fatty acid ratio index (PUFA:MUFA index) was derived from the pulse and collect spectra with water suppression, and comprised the resonance at δ2.80ppm (defined as the diallylic bond protons found in polyunsaturated fatty acids and denoted as “PUFA”) divided by the resonance at δ5.33ppm (-CH=CH- functional group, found in mono- and poly-unsaturated fatty acids, denoted as “MUFA”). The polyunsaturation index (PUI) was defined as the diallylic resonance divided by the sum of the allylic, diallylic, methyl and methylene resonances, expressed as a percentage[8]. Total choline (tCho) was derived from the pulse and collect spectra with water suppression and comprised the summed integral of the choline region resonances from δ3.18- δ3.28ppm, expressed as a percentage of the total spectral integral. The tCho region was further analysed using the CPMG data. Specifically, the resonance at δ3.26ppm, assigned as phosphatidylcholine (PtC) including contributions from betaine and trimethylamine-*N*-oxide (TMAO) and denoted as “PtC”, was compared to the tCho levels.

Significant differences in phenotypic data were sought by ANOVA testing with post-hoc Bonferroni analysis. Significant differences in MR spectral data were identified by the Kruskal-Wallis test or the Mann-Whitney U test as appropriate (SPSS v14.0, SPSS Inc. Chicago, USA).

Clinical Science Immediate Publication. Published on 12 Aug 2008 as manuscript CS20080159

Results

Phenotypic data

Body Weight

At baseline there was no significant difference in body mass between the inbred strains. However, as shown in Table 1, by 20 weeks there were significant differences in body mass both between the inbred strains and the dietary groups (ANOVA, $p<0.001$). Control diet (CD)-fed C3H mice gained weight more rapidly than CD-fed BALB/c animals (35.32±2.57g versus 26.49±0.87g; t-test, $p=0.006$) and HFD-fed C3H animals gained the greatest weight, being significantly heavier than either CD-fed littermates (44.72±0.34g versus 35.3±2.57g; $p=0.003$) or HFD fed BALB/c mice (27.52±0.70g; $p<0.001$). Indeed HFD-fed BALB/c gained little weight and were not significantly heavier than CD-fed BALB/c mice.

These differences increased during the course of the study with HFD-fed C3H animals being significantly heavier than all other groups at culling (55.24±0.80g versus C3H-CD 43.31±2.58g; $p=0.001$; BALB/c-HFD 35.29±1.11g; $p<0.001$). Whilst HFD-fed BALB/c mice began to increase in weight compared with control this did not reach statistical significance. Throughout the study, the weight of mutant Gena/263 mice was not significantly different to wild-type C3H mice fed the equivalent diet.

Glucose Tolerance

ANOVA analysis identified significant differences in blood glucose levels at all IPGTT time points (Table 1). HFD-fed C3H mice had significantly higher mean t=120 minute blood glucose concentrations than BALB/c mice fed HFD (11.86±0.96 versus 7.30±1.80 mmol/l, t-test, $p<0.001$). A trend towards impaired glucose tolerance was observed between HFD and CD-fed C3H animals but this did not reach statistical significance (11.86±0.96 versus 10.07±0.41 mmol/l). HFD fed Gena/263 mutant animals had significantly higher t=120 blood sugar levels than all other groups ($p<0.001$) including HFD-C3H mice (20.68±0.53 versus 11.86±0.96 mmol/l).

Histology

In keeping with the blunted weight gain and preservation of glucose tolerance in response to high fat diet, BALB/c mice were highly resistant to dietary induction of steatosis showing no histological evidence of steatosis in either CD or HFD groups at 36 weeks post-randomisation. In contrast, HFD fed C3H animals consistently exhibited a florid macro and micro-vesicular steatosis (median steatosis score 2/3) associated with ballooning hepatocyte degeneration (score 1/2) and a mild necroinflammatory infiltrate (score 1/3) (Table 1). Gena/263 mice exhibited mild spontaneous steatosis and a more moderate steatosis with some ballooning degeneration when fed HFD. A small but significant increase in serum ALT was observed between C3H dietary groups (HFD 47.60±4.41 versus CD 30.20±2.54 IU/L, $p=0.009$) and between HFD-fed C3H and BALB/c mice (47.60±4.41 versus 17.00±1.78 IU/L, $p=0.001$).

MR Characterisation

A representative water-supressed ^{1}H MAS-MR spectrum is shown in Figure 1 and illustrates the specific, quantifiable lipid resonances, including the fatty acid functional groups. The choline region (δ3.18-δ3.28ppm) contains four clearly identifiable peaks representing choline (δ3.20ppm), phosphocholine (PC) (δ3.22ppm), glycerophosphocholine (GPC) (δ3.23ppm) and PtC with contributions from TMAO and betaine at δ3.26ppm. Glucose and glycogen resonances were also prominent. A number of amino acid resonances were also visible.

Clinical Science Immediate Publication. Published on 12 Aug 2008 as manuscript CS20080159

The sum of the integrals for all lipid peaks was compared to the integral of the methylene lipid peak in all samples, demonstrating strong correlation between measures (Spearman rho correlation, r=0.998, p<0.0005). Accordingly, the integral of the methylene proton resonance was considered a surrogate for total lipid when describing lipid quantities relative to water.

Principal components analysis scores plots (data not shown) demonstrated clustering and separation of each mouse model from its control. This included the separation of models on the basis of diet (CD or HFD), strain (BALB/c and C3H, both on CD and HFD) and also presence of the Gena263 mutation from the wildtype control, both on CD and HFD.

Supervised PLS-DA models were then constructed. Correct class prediction was achieved with 100% accuracy for 6 of 7 comparisons of differing diet, strain and presence of the 263 mutation (Table 2).

Metabolites contributing to the spectral regions correlating strongly (positively or negatively) with each model compared to its control are documented in Table 3. Lipid moieties, choline-related compounds, glucose, glycogen and a number of amino acid resonances (including glutamine, leucine, lysine and alanine) were found to contribute to class separation. In particular, PtC (with contributions from betaine and TMAO) was found to be a major contributor to the PLS-DA models. Accordingly, PtC was integrated using the CPMG spectra and divided by the tCho region for comparison with histological class. The use of tCho as a denominator allowed relative quantitation of PtC without the potentially confounding dilutional effect of large changes in total lipid.

In addition to the separation of each model from its control, PLS-DA models were constructed to enable the classification of a single sample from the total dataset. 54 samples were included in the total dataset and class membership established with 100% accuracy in all but one model (Table 4).

Comparison between MAS MRS and histological assessment.

The distinction between simple steatosis and steatohepatitis is of importance for the development of models, which reflect progressive disease in humans. Therefore PCA was performed on spectra from mice of all strains fed HFD and stratified by histological assessment of NAFLD. The samples were divided into histologically normal, steatotic and steatohepatitic groups on the basis of histological assessment of an adjacent slice of tissue. Steatohepatitis was defined in this study as the presence of hepatocyte ballooning +/- the presence of necroinflammatory infiltrate. All samples in the steatohepatitis group had evidence of hepatocyte ballooning. PCA demonstrated clustering of the groups, so PLS-DA was performed to assess the factors associated with category membership. Category membership (between histologically normal, steatotic and steatohepatitic samples) using the leave-one-out algorithm was predicted with very high accuracy, as shown in Table 5.

The intrahepatic lipid level (median, interquartile range) differed significantly between samples histologically categorised as normal (1.96%, 1.02), steatosis (8.09%, 3.71) and steatohepatitis (10.56%, 6.08) (Figure 3A). There was a significant decrease in the PUFA:MUFA index between the normal (0.68, 0.09) and either steatotic (0.37, 0.12) or steatohepatitic (0.32, 0.09) samples. The PUFA:MUFA index did not differentiate

between the steatotic and steatohepatitic groups (Figure 3B). The PUI was decreased in steatotic (3.40%, 0.95) and steatohepatitic mice (2.95%, 1.13) compared to normal mice (6.29%, 1.25) (Mann-Whitney U test, $p<0.001$). Therefore, the increase in PUFA:MUFA index can be interpreted as consequent to a systematic decrease in PUFA with increasing disease severity. The resonances at δ3.26ppm (PtC with TMAO and betaine) and δ3.22-3.23ppm (PC and GPC) were found consistently to contribute to the difference between mouse classes on multivariate statistical modelling. tCho was significantly decreased in steatohepatitis (0.31%, 0.19) compared to steatosis (0.49%, 0.28) ($p=0.01$) and in both compared to the histologically normal samples (1.61%, 0.69) ($p<0.005$) (Figure 3C). Furthermore, PtC/tCho was significantly lower in the steatotic (33.7%, 16.8) and steatohepatitic animals (27.6%, 3.68) compared to normal animals (45.5%, 6.14) (Figure 3D). These findings are consistent with reports of low plasma PtC and high urinary choline oxidation products seen in 129S6 mice fed HFD[10].

Relationship between intrahepatic lipid and obesity in murine models

Mouse mass plotted against the %lipid:water (Figure 4A) demonstrated that intrahepatic lipid increased exponentially with increasing mouse mass at time of culling (R^2= 0.80, $p<0.0005$). The %lipid:water was also compared to the histological assessment of steatosis and demonstrated a close relationship between steatosis score and %lipid:water (Figure 4B).

Clinical Science Immediate Publication. Published on 12 Aug 2008 as manuscript CS20080159

Discussion

These data demonstrate that metabolic profiling of intact liver tissue using ^{1}H MAS MRS combined with PLS-DA is a powerful technique for the discrimination of NAFLD in animal models, differentiating by genetic (strain and the Gena/263 mutation), environmental (dietary) and histological factors. In particular, the first evidence is presented of accurate discrimination of histologically-defined steatosis and steatohepatitis using MRS of intact tissue. ^{1}H MAS MRS with PLS-DA also enables the separation and classification of different mouse strains on differing diets, despite normal histological appearances. Furthermore, it has been established that an exponential relationship exists between hepatic steatosis and obesity in these murine models.

In liver tissue, the "total signal" MR spectra are dominated by water and lipid resonances. Such spectra allow the quantitation of lipid, either in absolute terms, or as a proportion of the total signal in the spectrum. This marker of hepatic steatosis is a quantitative objective linear variable which compares favourably with the semi-quantitative subjective histological assessment of steatosis (Figures 4B)[7]. This is an important observation as steatosis is prerequisite for the development of steatohepatitis and consequent fibrotic liver disease. In HFD-fed animals, there was a progressive significant increase in the [%lipid:water] from normal through steatotic to steatohepatitic samples. This may represent increased uptake of fatty acids by the liver, decreased export or decreased catabolism[1]. Additionally, defective peripheral fatty acid uptake shunts more fatty acids to the liver[24]. Intrahepatic lipid increased exponentially with animal mass, suggesting that fatty acid uptake peripherally was maximised in these mice at a weight approaching 40g. Thereafter, intrahepatic lipid accumulated in preference to peripheral uptake of fatty acids and deposition of triacylglycerol (TAG). Accumulated free fatty acids may be disposed of by esterification to triglycerides and by fatty acid oxidation producing oxidative stress and initiating inflammation[25]. While the traditional two-hit hypothesis proposed that the development of steatosis is followed by a second hit initiating inflammation[26], recent work by Yamaguchi and colleagues suggests that this model is now too simple, and that visible lipid deposition is less pathogenically relevant[25]. Differential fatty acid partitioning between esterification, leading to the accumulation of visible fat and oxidation of the invisible FFA, is more relevant to the pathogenesis. The use of MRS techniques in this study enables the determination of *total* lipid composition, which includes the assessment of the invisible hepatic FFA component.

The relative decrease in PUFA seen with increasing disease severity supports previous evidence, that a decrease in PUFAs has been observed in in the liver and blood of obese Zucker rats[9] and in the serum of human subjects with hepatic steatosis and steatohepatitis[27;28]. A reduced PUFA:MUFA ratio has been considered to represent a surrogate marker of lipid peroxidation, associated with oxidative stress[9]. Depletion of long chain PUFA (LC-PUFA) within the liver is thought to increase FA and TAG synthesis by upregulation of lipogenic genes via reduced downregulation of sterol regulatory binding protein (SREBP-1), and to decrease FA oxidation, including by a reduction of PPAR-α activation[29].

PtC is an essential phospholipid[30], existing as a membrane-bound macromolecule giving rise to a broad resonance[31] within which the -$N(CH_3)_3$ functional group of trimethylamine-N-oxide (TMAO) and betaine (oxidation products of choline metabolism) are co-resonant[16]. Measurement of choline levels demonstrates a decrease in choline-containing products in the obese models, and in those animals with steatosis and

steatohepatitis, compared to histologically normal controls. Importantly, the tCho is significantly lower in steatohepatitis compared to simple steatosis. This is consistent with the observation that mice fed a choline-deficient diet develop hepatic steatosis and steatohepatitis[32]. However, increasing lipid, which dominates the spectrum, may also contribute to the reduction in tCho observed, by means of a dilution effect. Therefore, the PtC resonance (also containing betaine and TMAO) was integrated in isolation and expressed as a ratio of the total choline region. PtC biosynthesis from choline and methionine is required for normal hepatic secretion of VLDL[33], and decreased PtC leads to accumulation of intracellular triglyceride[34]. Indeed, when comparing the PtC resonance to the total choline region, PtC is reduced compared to other choline-containing products in mice with hepatic steatosis and steatohepatitis compared to histologically normal livers. This is consistent with work on aqueous liver tissue extract in obese Zucker rats: a reduction in betaine at δ3.26 compared to lean controls[9] has been shown to protect against alcoholic hepatic steatosis in experimental animals[35].

As with any technique, there are limitations to this approach to studying NALFD. While ^{1}H MAS MRS allows the quantitation of protons within functional groups of metabolites, it is not possible directly to quantify specific fatty acids, as this requires accurate measurement of fatty acyl chain length and the position and number of functional groups within the chain. Nevertheless, the extent of saturation or (poly)unsaturation is of biological and clinical relevance. The overlap of certain resonances (particularly small resonances near the larger lipid peaks) may reduce the accuracy of integration of those peaks. However, by dividing the spectra into small regions or “buckets”, quantitation is objective and consistent. Curve-fitting software is used in the *in vivo* setting and enables quantitation of small numbers of overlapping peaks. Newer approaches such as “targeted profiling” may improve quantitation of the multiple peaks found in complex tissue and biofluid samples *in vitro*[36].

This study has demonstrated that a small number of resonances contribute reliably to the differentiating the cohorts studied. Despite low field strength and the presence of motion artefact, tCho and a number of lipid resonances may be resolved in human liver *in vivo*[37], raising the possibility that ^{1}H MRS could provide discriminatory information in the context of NAFLD *in vivo*.

In conclusion, this study has demonstrated the utility of ^{1}H MAS MRS of intact liver tissue in conjunction with multivariate modelling techniques for the investigation and classification of murine models of NAFLD on the basis of environmental, genetic and histopathological features. Class membership may be predicted with high accuracy and it is possible to distinguish reliably between samples, even where histological appearances are indistinguishable. PLS-DA enables the identification of biologically-relevant metabolites contributing to the differences between models. Future studies may employ these techniques to screen the output of programs generating murine models of NAFLD and other liver diseases. Greater subject numbers will facilitate the use of separate large training and test sets. High resolution ^{1}H MAS MRS data may be used to aid the interpretation of future non-invasive *in vivo* MRS studies. As the resolution of ^{1}H MR spectra from *in vivo* MR scanners improves, combination with multivariate statistical analysis may allow detailed non-invasive assessment of hepatic disease in animals and humans.

Acknowledgements
J.F.L.C holds the Centenary Fellowship from the Hammersmith Hospitals Trustees Research Committee. Q.M.A. is a Medical Research Council funded Clinical Research Fellow. H.R.T.W is funded by the Broad Medical Research Program, USA. H.C.M holds a Research Training Fellowship from the Wellcome Trust. H.C.T, S.D.T-R, M.R.T and I.J.C are grateful for support from the NIHR Biomedical Research Centre funding scheme.

References

1. Anstee,Q.M. and Goldin,R.D. (2006) Mouse models in non-alcoholic fatty liver disease and steatohepatitis research. Int.J.Exp.Pathol. **87**, 1-16.

2. Marchesini,G., Brizi,M., Morselli-Labate,A.M. et al. (1999) Association of nonalcoholic fatty liver disease with insulin resistance. Am.J Med. **107**, 450-455.

3. Powell,E.E., Cooksley,W.G., Hanson,R., Searle,J., Halliday,J.W. and Powell,L.W. (1990) The natural history of nonalcoholic steatohepatitis: a follow-up study of forty-two patients for up to 21 years. Hepatology **11**, 74-80.

4. Sanyal,A.J. (2002) AGA technical review on nonalcoholic fatty liver disease. Gastroenterology **123**, 1705-1725.

5. Koteish,A. and Mae,D.A. (2002) Animal models of steatohepatitis. Best.Pract.Res.Clin.Gastroenterol. **16**, 679-690.

6. Angulo,P. (2002) Nonalcoholic fatty liver disease. N.Engl.J.Med. **346**, 1221-1231.

7. Szczepaniak,L.S., Nurenberg,P., Leonard,D. et al. (2005) Magnetic resonance spectroscopy to measure hepatic triglyceride content: prevalence of hepatic steatosis in the general population. Am.J.Physiol Endocrinol.Metab **288**, E462-E468.

8. Johnson,N.A., Walton,D.W., Sachinwalla,T. et al. (2008) Noninvasive assessment of hepatic lipid composition: Advancing understanding and management of fatty liver disorders. Hepatology **47**, 1513-1523.

9. Serkova,N.J., Jackman,M., Brown,J.L. et al. (2006) Metabolic profiling of livers and blood from obese Zucker rats. J.Hepatol. **44**, 956-962.

10. Dumas,M.E., Barton,R.H., Toye,A. et al. (2006) Metabolic profiling reveals a contribution of gut microbiota to fatty liver phenotype in insulin-resistant mice. Proc.Natl.Acad.Sci.U.S.A **103**, 12511-12516.

11. Fearnside,J.F., Dumas,M.E., Rothwell,A.R. et al. (2008) Phylometabonomic patterns of adaptation to high fat diet feeding in inbred mice. PLoS.ONE. **3**, e1668.

12. Bollard,M.E., Garrod,S., Holmes,E. et al. (2000) High-resolution (1)H and (1)H-(13)C magic angle spinning NMR spectroscopy of rat liver. Magn Reson.Med. **44**, 201-207.

13. Dave,U., Taylor-Robinson,S.D., Walker,M.M. et al. (2004) In vitro 1H-magnetic resonance spectroscopy of Barrett's esophageal mucosa using magic angle spinning techniques. Eur.J.Gastroenterol.Hepatol. **16**, 1199-1205.

14. Duarte,I.F., Stanley,E.G., Holmes,E. et al. (2005) Metabolic assessment of human liver transplants from biopsy samples at the donor and recipient stages

using high-resolution magic angle spinning 1H NMR spectroscopy. Anal.Chem. **77**, 5570-5578.

15. Martinez-Granados,B., Monleon,D., Martinez-Bisbal,M.C. et al. (2006) Metabolite identification in human liver needle biopsies by high-resolution magic angle spinning 1H NMR spectroscopy. NMR Biomed. **19**, 90-100.

16. Rooney,O.M., Troke,J., Nicholson,J.K. and Griffin,J.L. (2003) High-resolution diffusion and relaxation-edited magic angle spinning 1H NMR spectroscopy of intact liver tissue. Magn Reson.Med. **50**, 925-930.

17. Bertram,H.C., Duarte,I.F., Gil,A.M., Knudsen,K.E. and Laerke,H.N. (2007) Metabolic profiling of liver from hypercholesterolemic pigs fed rye or wheat fiber and from normal pigs. High-resolution magic angle spinning 1H NMR spectroscopic study. Anal.Chem. **79**, 168-175.

18. Matthews, H. C., Absalom, N., Goldsworthy, M., Thomas, H. C., Goldin, R., Thursz, M. R., and Cox, R. Buttermouse:the effect of high fat feeding on a new mouse model of insulin resistance and steatohepatitis. Journal of Hepatology **46**, S276. 2007.

19. Kleiner,D.E., Brunt,E.M., Van,N.M. et al. (2005) Design and validation of a histological scoring system for nonalcoholic fatty liver disease. Hepatology **41**, 1313-1321.

20. Mahon,M.M., Cox,I.J., Dina,R. et al. (2004) (1)H magnetic resonance spectroscopy of preinvasive and invasive cervical cancer: in vivo-ex vivo profiles and effect of tumor load. J.Magn Reson.Imaging **19**, 356-364.

21. Gavaghan,C.L., Wilson,I.D. and Nicholson,J.K. (2002) Physiological variation in metabolic phenotyping and functional genomic studies: use of orthogonal signal correction and PLS-DA. FEBS Lett. **530**, 191-196.

22. Jones,G.L., Sang,E., Goddard,C. et al. (2005) A functional analysis of mouse models of cardiac disease through metabolic profiling. J.Biol.Chem. **280**, 7530-7539.

23. Westerhuis,J.A., Hoefsloot,H.C.J., Smit,S. et al. (2008) Assessment of PLSDA cross validation. Metabolomics **4**, 81-89.

24. Goldberg,I.J. and Ginsberg,H.N. (2006) Ins and outs modulating hepatic triglyceride and development of nonalcoholic fatty liver disease. Gastroenterology **130**, 1343-1346.

25. Yamaguchi,K., Yang,L., McCall,S. et al. (2007) Inhibiting triglyceride synthesis improves hepatic steatosis but exacerbates liver damage and fibrosis in obese mice with nonalcoholic steatohepatitis. Hepatology **45**, 1366-1374.

26. Day,C.P. and James,O.F. (1998) Steatohepatitis: a tale of two "hits"? Gastroenterology **114**, 842-845.

27. Puri,P., Baillie,R.A., Wiest,M.M. et al. (2007) A lipidomic analysis of nonalcoholic fatty liver disease. Hepatology **46**, 1081-1090.

28. Elizondo,A., Araya,J., Rodrigo,R. et al. (2007) Polyunsaturated fatty acid pattern in liver and erythrocyte phospholipids from obese patients. Obesity.(Silver.Spring) **15**, 24-31.

29. Videla,L.A., Rodrigo,R., Araya,J. and Poniachik,J. (2004) Oxidative stress and depletion of hepatic long-chain polyunsaturated fatty acids may contribute to nonalcoholic fatty liver disease. Free Radic.Biol.Med. **37**, 1499-1507.

30. Li,Z. and Vance,D.E. (2008) Phosphatidylcholine and choline homeostasis. J.Lipid Res. **49**, 1187-1194.

31. Millis,K., Weybright,P., Campbell,N. et al. (1999) Classification of human liposarcoma and lipoma using ex vivo proton NMR spectroscopy. Magn Reson.Med. **41**, 257-267.

32. Walkey,C.J., Yu,L., Agellon,L.B. and Vance,D.E. (1998) Biochemical and evolutionary significance of phospholipid methylation. J.Biol.Chem. **273**, 27043-27046.

33. Yao,Z.M. and Vance,D.E. (1988) The active synthesis of phosphatidylcholine is required for very low density lipoprotein secretion from rat hepatocytes. J.Biol.Chem. **263**, 2998-3004.

34. Noga,A.A., Zhao,Y. and Vance,D.E. (2002) An unexpected requirement for phosphatidylethanolamine N-methyltransferase in the secretion of very low density lipoproteins. J.Biol.Chem. **277**, 42358-42365.

35. Kharbanda,K.K., Mailliard,M.E., Baldwin,C.R., Beckenhauer,H.C., Sorrell,M.F. and Tuma,D.J. (2007) Betaine attenuates alcoholic steatosis by restoring phosphatidylcholine generation via the phosphatidylethanolamine methyltransferase pathway. J.Hepatol. **46**, 314-321.

36. Weljie,A.M., Newton,J., Mercier,P., Carlson,E. and Slupsky,C.M. (2006) Targeted profiling: quantitative analysis of 1H NMR metabolomics data. Anal.Chem. **78**, 4430-4442.

37. Fischbach,F. and Bruhn,H. (2008) Assessment of in vivo 1H magnetic resonance spectroscopy in the liver: a review. Liver Int. **28**, 297-307.

Figure 1.

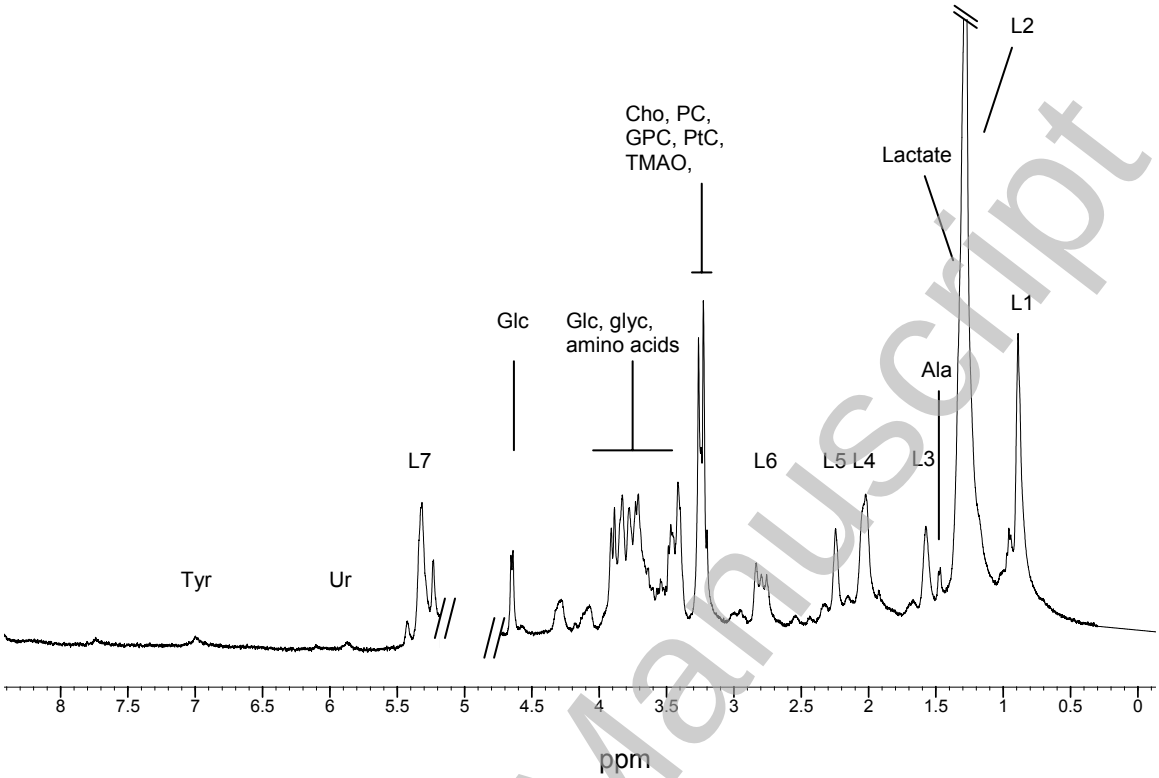

Figure 1. Water-suppressed, fully relaxed ^{1}H MAS-MR spectrum from a C3H mouse on CD. The residual water resonance at δ4.8-5.2 was removed as indicated. Key: L1, lipid $\mathbf{CH_3}CH_2$ (methyl); L2 lipid $(\mathbf{CH_2})_n$ (methylene); L3 lipid $\mathbf{CH_2}CH_2CO$ (methylene to L5); L4 lipid $CH{=}CH\mathbf{CH_2}CH_2$ (allylic); L5 lipid $CH_2\mathbf{CH_2}CO$ (α-methylene to carboxyl); L6 lipid $CH{=}CH\mathbf{CH_2}CH{=}CH$ (diallylic- "PUFA"); L7 lipid **CH=CH** (methene- "MUFA"); Ala, alanine; Cho, choline; PC, phosphocholine; GPC, glycerophosphocholine; PtC, phosphatidylcholine; TMAO, trimethylamine-N-oxide; Glc, glucose; Glyc, glycogen; Urd, uridine; Tyr, tyrosine.

Clinical Science Immediate Publication. Published on 12 Aug 2008 as manuscript CS20080159

Figure 2.

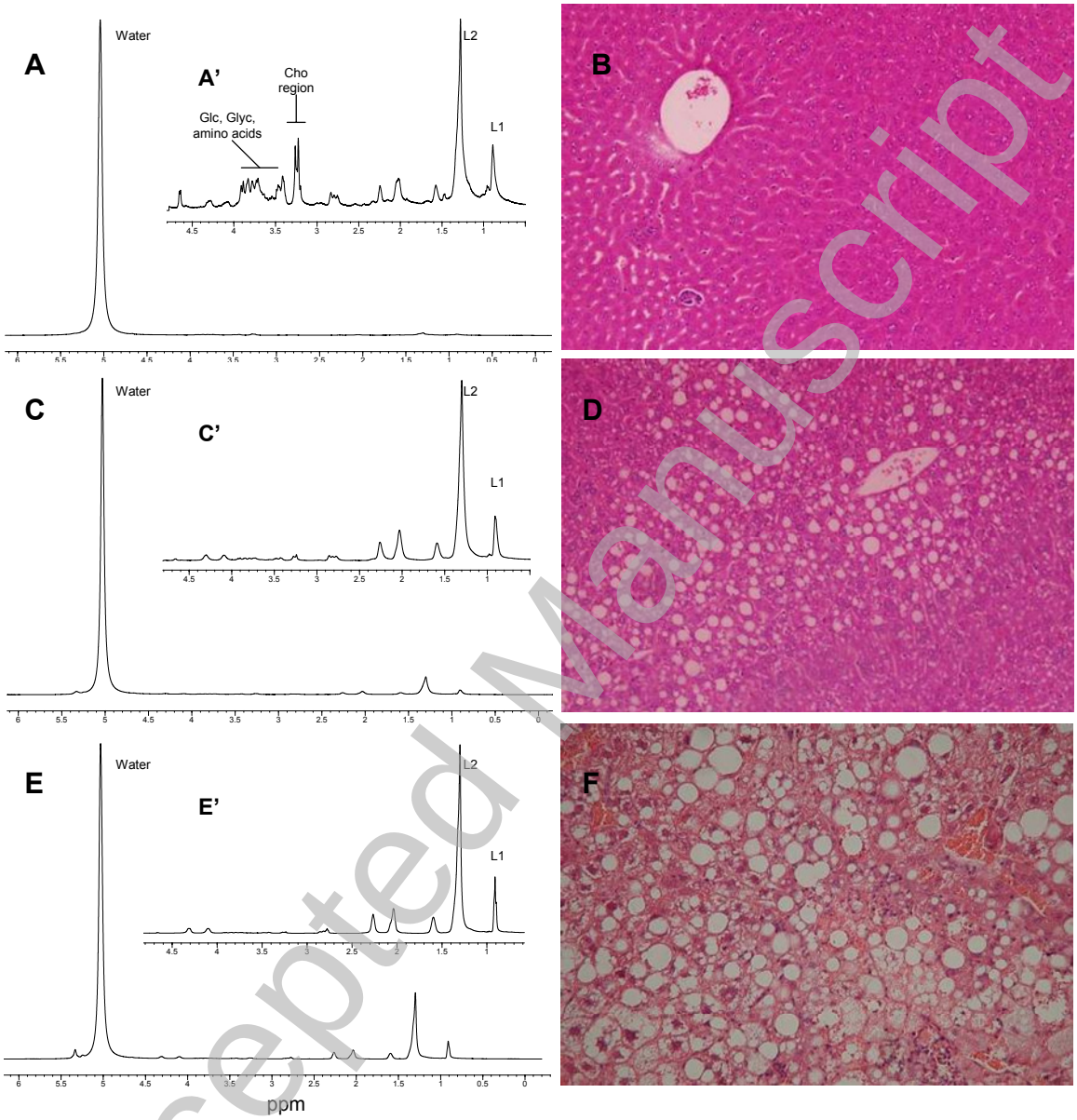

Clinical Science Immediate Publication. Published on 12 Aug 2008 as manuscript CS20080159

Figure 2. Figure shows representative ^{1}H MAS MRS spectra without and with water suppression, with paired histology from samples with normal architecture (A, A' and B), steatosis (C, C' and D) and steatohepatitis (E, E' and F). The "total signal" MR spectra (A, C, E) illustrate the ratio of water to other metabolites. The "lipid signal" MR spectra (A', C', E') amplify other major metabolite groups. The lipid consituents increase, while the tCho decreases with increasing disease severity. Characteristic histological features of steatosis (lipid droplets) and steatohepatitis (hepatocyte ballooning) from the corresponding tissue sample are shown in D and F.

Clinical Science Immediate Publication. Published on 12 Aug 2008 as manuscript CS20080159

Figure 3.

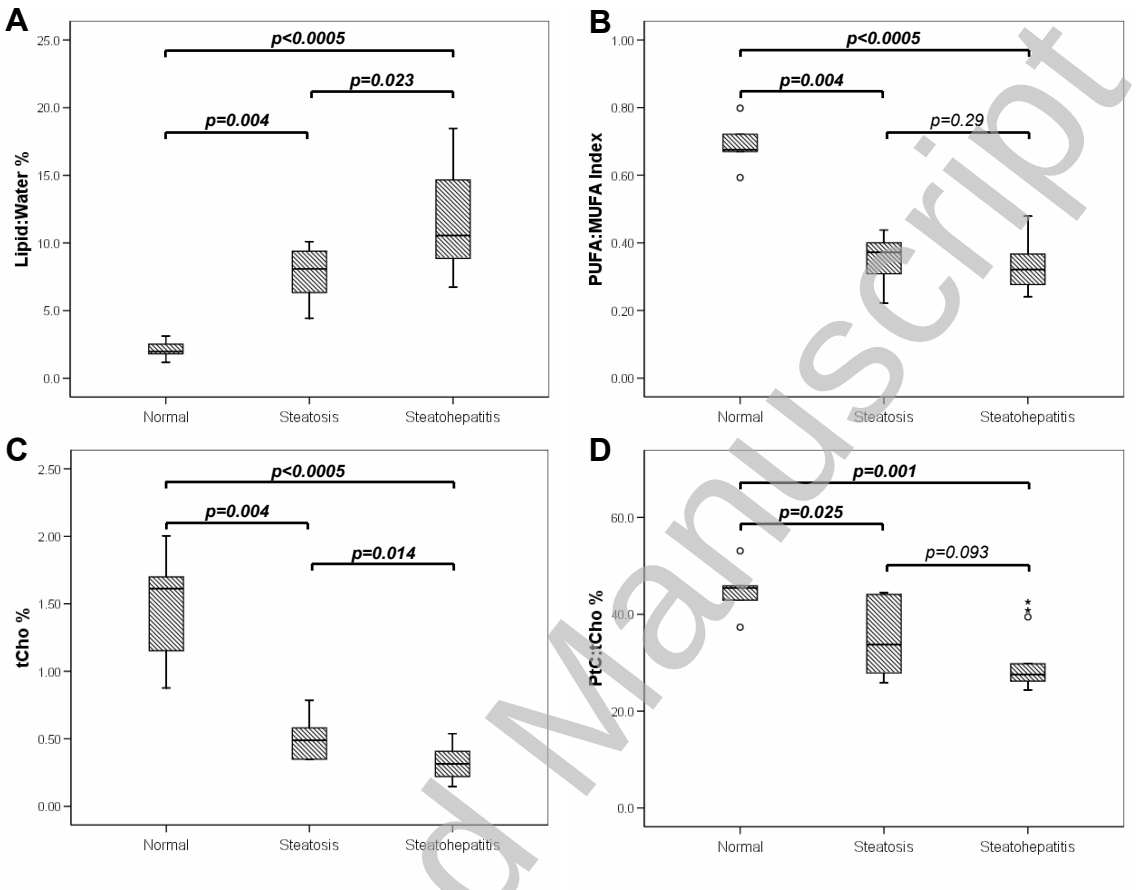

Figure 3. "Box and whisker" plot demonstrating the differences in key metabolite ratios between histologically normal, steatotic and steatohepatitic samples on HFD. **A** shows the lipid:water ratio, consisting of the methylene functional group resonance expressed as a percentage of water. **B** shows the PUFA:MUFA ratio index. **C** shows the tCho level; **D** shows the PtC:tCho. p- values for the Mann-Witney U test are stated (in bold for significance at the 95% level).

Clinical Science Immediate Publication. Published on 12 Aug 2008 as manuscript CS20080159

Figure 4.

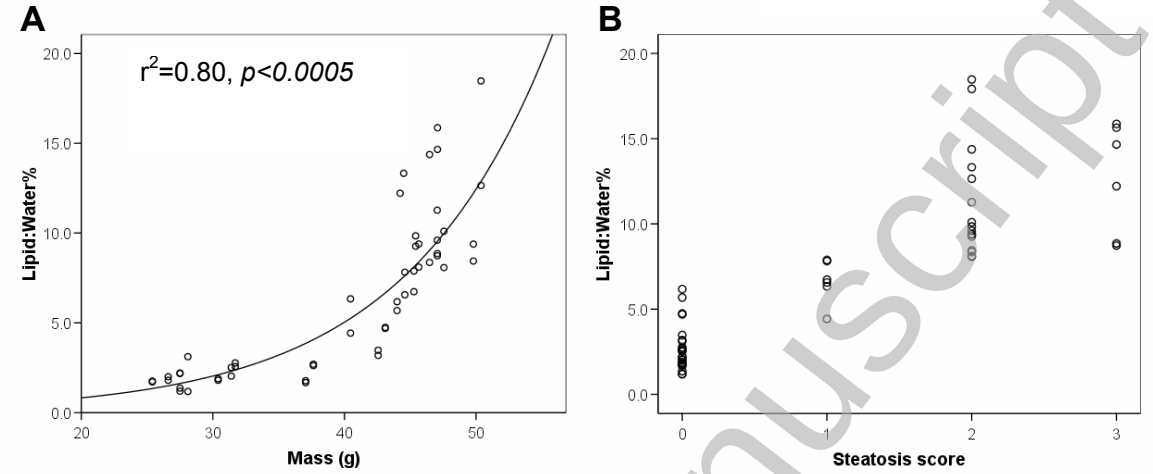

Figure 4. Scatter graphs showing the lipid:water ratio plotted against A) the mass of mouse in grams and B) the histological steatosis score.

Clinical Science Immediate Publication. Published on 12 Aug 2008 as manuscript CS20080159

Table 1. Phenotype of mice and effects of the high fat diet (HFD).

		Mean Body Weight /g (SEM)†			*Mean IPGTT at 12 Weeks /mmol/L (SEM)*			*Median NAS Score**			*Hist.*
		6 Weeks	**20 Weeks**	**36 Weeks**	**T=0**	**T=60**	**T=120**	**St.**	**Fib.**	**Inf.**	**Ball.**
C3H	**Control**	25.38 (0.59)	35.32 (2.58)	43.31 (2.58)	6.83 (0.22)	15.38 (1.94)	10.07 (0.41)	0	0	0	0
	HFD	25.24 (0.23)	44.72 (0.34)	55.24 (0.80)	10.42 (0.53)	21.26 (1.17)	11.86 (0.96)	2	0	1	1
BALB/c	**Control**	24.29 (0.83)	26.49 (0.87)	31.40 (1.53)	4.47 (0.99)	16.13 (2.48)	7.66 (1.52)	0	0	0	0
	HFD	23.25 (0.89)	27.52 (0.70)	35.29 (1.11)	3.58 (0.20)	11.34 (2.87)	7.30 (1.80)	0	0	0	0
		6 Weeks	***20 Weeks***	***36 Weeks***	***Mean IPGTT at 12 Weeks /mmol/L (SEM)***			***Median NAS Score****			***Hist.***
					T=0	**T=60**	**T=120**	**St.**	**Fib.**	**Inf.**	**Ball.**
Gena/263	**Control**	24.56 (1.2)‡	41.60 (2.06)	-	10.84 (1.81)	26.66 (2.13)	22.43 (1.27)	1	0	0	2
	HFD	25.38 (0.46)	45.50 (0.64)	-	9.31 (0.95)	28.65 (1.42)	20.68 (0.53)	3	0	0	1
Non-Mut	**Control**	27.89 (0.5)‡-	42.40 (2.57)	-	5.22 (1.93)	11.67 (0.29)	8.15 (1.14)	0	0	0	0
	HFD	26.58 (0.33)	44.76 (0.79)	-	8.42 (0.65)	23.43 (0.86)	13.30 (0.36)	2	0	0	1

Table 1. Phenotype of mice and effects of the high fat diet (HFD) on body mass, glucose tolerance and histological scoring are tabulated. † Weight recorded at start of experiment (age 6 weeks), mid-experiment and at cull point. BALB/c and C3H were culled at 36 weeks, Gena/263 mice (and C3H controls) were culled at 20 weeks.
‡ 6 week control diet data from separate cohort of animals to those used in MRS study, shown for illustrative purposes.
* NAS Score: Steatosis (0-3), Fibrosis (0-4), Inflammation (0-3), Ballooning Hepatocyte degeneration (0-2).

Clinical Science Immediate Publication. Published on 12 Aug 2008 as manuscript CS20080159

Table 2. A comparison of each model against its control in dataset. PLS-DA models were constructed to separate the MR spectra obtained from a given mouse model from its control as specified, with one orthogonal factor removed (OSC).

Model	Control	Components	Correct prediction of model	Correct prediction of control	Incorrect prediction of model (false positive)	No match	Q^2
BALB/c HFD	BALB/c CD	1	6/6	6/6	-	-	0.998
C3H HFD	C3H CD	1	6/6	6/6	-	-	0.898
Gena/263 HFD	Gena/263 CD	2	8/8	6/6	-	-	0.877
C3H CD	BALB/c CD	1	6/6	6/6	-	-	0.996
C3H HFD	BALB/c HFD	1	6/6	6/6	-	-	0.917
Gena/263 CD	Non-mut CD	1	6/6	6/6	-	-	0.982
Gena/263 HFD	Non-mut HFD	1	8/8	8/10	1	1	0.460

Clinical Science Immediate Publication. Published on 12 Aug 2008 as manuscript CS20080159

Table 3. Table of main differences in metabolites contributing to the discrimination of classes between different murine models. Where specified, the amino acid cluster includes resonances including leucine, alanine, lysine and glutamine.

Model	Control	Primary discriminator	Major discriminators (order of decreasing influence on model)
BALB/c HFD	BALB/c CD	Lipid C**H**$_2$	PtC, β-glucose, amino acids
C3H HFD	C3H CD	Lipid C**H**$_2$	Lipid C**H**=C**H**, PtC, lipid **CH**$_2$CH$_2$CO
Gena/263 HFD	Gena/263 CD	Lipid C**H**=C**H**	Lipid C**H**$_3$, β-glucose, PtC
C3H CD	BALB/c CD	Lipid C**H**$_2$	PtC, α and β glucose, amino acids
C3H HFD	BALB/c HFD	α and β glucose	Lipid C**H**$_2$, PtC, amino acids lipid C**H**$_3$
Gena/263 CD	Non-mut CD	PtC	Lipid C**H**$_2$, α glucose, amino acids, glucose, PC, lipid C**H**=C**H**
Gena/263 HFD	Non-mut HFD	lipid C**H**=C**H**	lipid CH$_3$, α and β glucose, amino acids

Clinical Science Immediate Publication. Published on 12 Aug 2008 as manuscript CS20080159

Table 4. A comparison of each group against all mice in dataset. Each PLS-DA model (from which 2 orthogonal factors had been removed, OSC) was constructed to separate the MR spectra obtained from a given mouse model from all other samples of all models in the total dataset.

Model	Diet	Components	Correct prediction of model	Correct prediction of non-fit	Incorrect prediction of model	No match	Q^2
BALB/c	CD	2	4/6	48/48	-	2	0.994
	HFD	5	6/6	48/48	-	-	0.996
C3H	CD	5	6/6	48/48	-	-	0.761
	HFD	3	6/6	48/48	-	-	0.998
Non-mut	CD	3	5/6	48/48	-	1	0.996
	HFD	3	10/10	44/44	-	-	0.996
Gena/263	CD	2	6/6	48/48	-	-	0.994
	HFD	2	8/8	46/46	-	-	0.977

Clinical Science Immediate Publication. Published on 12 Aug 2008 as manuscript CS20080159

Table 5. A comparison of histologically normal, steatotic, and steatohepatitic samples from the HFD dataset. The PLS-DA model with OSC was constructed to separate the MR spectra obtained from a given category from all other samples of the other categories in the dataset.

Histological category	Components	Correct prediction of model	Correct prediction of non-fit	Incorrect prediction of model	No match	Q^2
Normal	3	5/6	24/24	-	1	0.997
Steatosis	3	6/6	24/24	-	-	0.996
Steatohepatitis	3	18/18	12/12	-	-	0.999